THE UNIVERSITY OF RHODE ISLAND

Graduate School of Oceanography Faculty Publications

Graduate School of Oceanography

2007

Seasonal Variability of the South Equatorial Current Bifurcation in the Atlantic Ocean: A Numerical Study

Regina R. Rodrigues

Lewis M. Rothstein

Mark Wimbush
University of Rhode Island

Seasonal Variability of the South Equatorial Current Bifurcation in the Atlantic Ocean: A Numerical Study

Seasonal Variability of the South Equatorial Current Bifurcation in the Atlantic Ocean: A Numerical Study

REGINA R. RODRIGUES,* LEWIS M. ROTHSTEIN, AND MARK WIMBUSH

Graduate School of Oceanography, University of Rhode Island, Narragansett, Rhode Island

ABSTRACT

In this study, a reduced-gravity, primitive equation OGCM is used to investigate the seasonal variability of the bifurcation of the South Equatorial Current (SEC) into the Brazil (BC) to the south and the North Brazil Undercurrent/Current (NBUC/NBC) system to the north. Annual mean meridional velocity averaged within a 2° longitude band off the South American coast shows that the SEC bifurcation occurs at about 10°–14°S near the surface, shifting poleward with increasing depth, reaching 27°S at 1000 m, in both observations and model. The bifurcation latitude reaches its southernmost position in July (~17°S in the top 200 m) and its northernmost position in November (~13°S in the top 200 m). The model results show that most of the seasonal variability of the bifurcation latitude in the upper thermocline is associated with changes in the local wind stress curl due to the annual north–south excursion of the marine ITCZ complex. As the SEC bifurcation latitude moves south (north) the NBUC transport increases (decreases) and the BC transport decreases (increases). The remote forcing (i.e., westward propagation of anomalies) appears to have a smaller impact on the seasonal variability of the bifurcation in the upper thermocline.

1. Introduction

The South Equatorial Current (SEC) forms the northern part of the South Atlantic Ocean subtropical gyre, carrying subtropical water from the Benguela Current region toward the Brazil shelf region around 14°S, where it bifurcates into the North Brazil Undercurrent (NBUC) to the north and the Brazil Current (BC) to the south. The SEC bifurcation can have implications on the climate variability because the SEC/NBUC system is the main conduit for upper-ocean return flow of the meridional overturning circulation (MOC) (Talley 2003; Ganachaud 2003; Lumpkin and Speer 2003) and for the subtropical–tropical mass exchange [the subtropical cells (STC)] (Malanotte-Rizzoli et al. 2000; Zhang et al. 2003). In the Atlantic Ocean, most of the water encountered in the equatorial thermocline comes from the South Atlantic through the

low-latitude western boundary current, which is the NBUC/North Brazil Current (NBC); see for example, Metcalf and Stalcup (1967), Wilson et al. (1994), Schott et al. (1995), Zhang et al. (2003), and Goes et al. (2005) from observations; Harper (2000), Malanotte-Rizzoli et al. (2000), Inui et al. (2002), Lazar et al. (2002), and Hazeleger et al. (2003) from model results. The bifurcation latitude could be indicative of the amount of subtropical water imported to the Tropics and to the North Atlantic via the NBUC/NBC and the amount of it that recirculates in the subtropical gyre. Moreover, the variability in the bifurcation latitude and in the transport of the currents can impact other remote regions downstream of the NBUC and BC, for instance the NBC rings (Johns et al. 2003) and the Brazil–Malvinas confluence (Vivier and Provost 1999) regions, respectively.

The determination of the SEC bifurcation latitude still remains obscure for the South Atlantic. A crude estimate of the bifurcation latitude can be obtained from the position of the zero line of zonally integrated wind stress curl, that is, the Sverdrup theory. For instance, this theory predicts that the latitude of the SEC bifurcation at the coast of South America should be 14°S, which coincides with the northern edge of the South Atlantic subtropical gyre [using the Comprehensive Ocean–Atmosphere Data Set (COADS) wind

---

* Current affiliation: NOAA/Pacific Marine Environmental Laboratory, Seattle, Washington.

Corresponding author address: Regina R. Rodrigues, NOAA/Pacific Marine Environmental Laboratory, Bldg. 3, 7600 Sand Point Way NE, Seattle, WA 98115.
E-mail: regina.rodrigues@noaa.gov

dataset; da Silva et al. 1994]. Previous observational studies of the South Atlantic circulation suggest that the SEC bifurcation occurs at 14°–16°S in the surface layer (0–100 m), at 20°–24°S in the thermocline (400–500 m), and at 26°–28°S in the intermediate layer (600–1200 m) (Stramma and England 1999; Boebel et al. 1999; Wienders et al. 2000). From numerical model results, the bifurcation point in the near-surface layer at the western boundary of the South Atlantic occurs at 18°S in the simulations by Harper (2000) and at 17°S in those by Malanotte-Rizzoli et al. (2000).

No attempt has been made to explain the mechanisms involved in the SEC bifurcation process that dictate its position and the partition between waters flowing poleward and those flowing equatorward. The aforementioned studies are rather descriptive of the SEC bifurcation. However, relevant to the present work a number of studies have been developed for the bifurcation of the North Equatorial Current (NEC) in the Pacific Ocean. Qiu and Lukas (1996) tried unsuccessfully to relate the seasonal variability of the NEC bifurcation to the annual meridional excursion of the zero line of zonally integrated wind stress curl. Later, Qu and Lukas (2003) and Kim et al. (2004) found that the seasonal variability of the NEC is strongly correlated to the local Ekman pumping associated with the monsoonal winds, which are superimposed on the basinwide wind system. The zero line of zonally integrated wind stress curl fails to explain the seasonal variation of the bifurcation because it only gives an estimate of the bifurcation latitude for a steady-state barotropic ocean (Sverdrup model). As pointed out by Qu and Lukas (2003), the steady-state, depth-averaged Sverdrup theory does not consider the interactions and exchanges of water masses between the tropical and subtropical gyres, nor the depth dependence of the subtropical gyre circulation and thus of the bifurcation latitude. Moreover, the wind forcing strongly varies both spatially and temporally in the South Atlantic; the seasonal signal is particularly strong. This is expected to impact the bifurcation of the SEC locally (through Ekman transports) and remotely (through the propagation of Rossby waves generated by basinwide winds), similar to what Kim et al. (2004) found for the Pacific NEC.

The main objective of the present study is to provide a detailed description of the SEC bifurcation and investigate its seasonal variability. To address that, an upper-ocean reduced-gravity multilayer model (Chen et al. 1994a,b; Gent and Cane 1989) is used. The model has already proven to be a useful tool in analyzing the subtropical cells and subduction pathways in the Pacific, Indian, and Atlantic Oceans (Chen et al. 1994b; Rothstein et al. 1998; Inui et al. 2002; Lazar et al. 2001,

2002). In addition, an annual mean climatology of temperature and salinity is constructed from observations to validate the model results in terms of the annual-mean depth dependence of the SEC bifurcation. This work is organized as follows. Section 2 briefly describes the numerical model and temperature and salinity climatology. Section 3 presents the observational and numerical results and addresses the seasonal variability of the SEC bifurcation. Section 4 contains a summary and the main conclusions.

2. Methods

a. Observations

The observations used here are quality-controlled CTD and bottle data obtained from HydroBase (Curry 1996) for the South Atlantic within the region 0°–30°S, 50°–10°W (3284 casts, see black dots in Fig. 1). Only stations that reach deeper than 1000 dbar were used and bottle data with less than six samples in the main thermocline were eliminated. The temperature and salinity data were then linearly interpolated at 25-dbar intervals and used to calculate dynamic heights relative to 1000 dbar, from which geostrophic velocities were determined. The dynamic heights were first averaged into $1° \times 1°$ bins for all pressure levels. Typical dynamic height standard deviations range from 0.3 $m^2 s^{-2}$ at the surface to 0.033 $m^2 s^{-2}$ at 900 m. The resulting bin-averaged data are then interpolated using a multivariate objective analysis, according to Watts et al. (2001), with *e*-folding scales of 2° latitude–longitude. Although the requirement of retaining only casts deeper than 1000 dbar restricts the number of observations used in this analysis, it allows calculating the dynamic heights before gridding them. This procedure avoids gridding the temperature and salinity data on different pressure levels using different grid resolutions, as in Qu and Lukas (2003).

b. Numerical model

The upper-ocean, reduced-gravity, multilayer model is a version of the primitive equation, sigma-coordinate model developed by Gent and Cane (1989), with the embedded hybrid vertical mixing submodel of Chen et al. (1994a). This mixing model incorporates physics of the Kraus and Turner (1967) mixed layer model and the Price et al. (1986) dynamical instability model, as well as an instantaneous convective adjustment. By combining the advantages of these two models, the hybrid scheme simulates the three major physical processes of oceanic vertical turbulent mixing in a computationally efficient manner (Chen et al. 1994a,b). The mixed layer
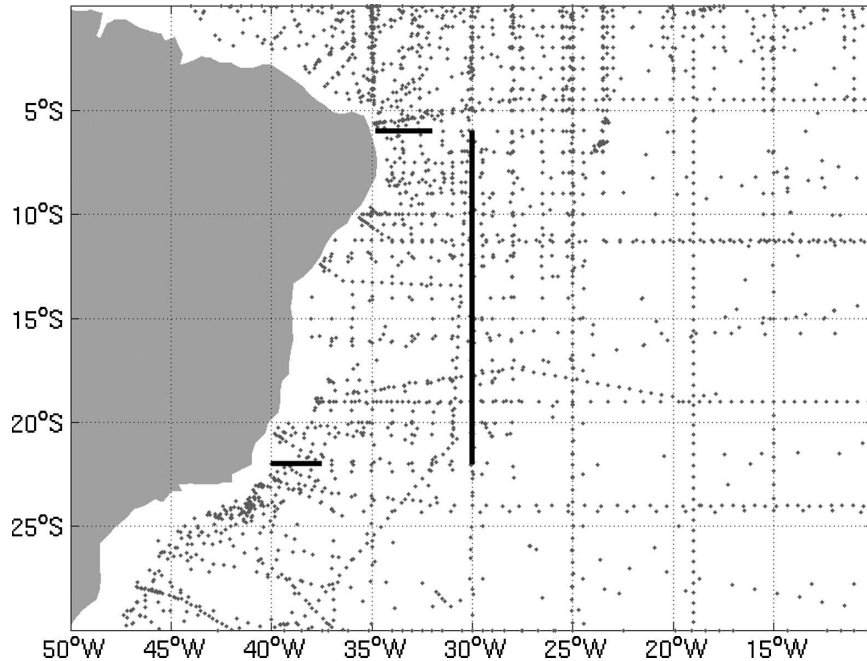
FIG. 1. Selected hydrographic stations used to calculate dynamic height referenced to 1000 dbar and geostrophic current (total of 3284 casts). Solid black lines represent transects for the calculation of NBUC, SEC, and BC transports.

entrainment and detrainment are related to atmospheric forcing using a bulk mixed layer model; the shear flow instability is accounted for by partial mixing controlled by the gradient Richardson number; and free convection in the thermocline is simulated by an instantaneous adjustment. One of the main features of this model is its ability to reproduce accurately the mixed layer, a key factor for this study. More details about the model formulation can be found in Ginis et al. (1998).

The model domain extends from 50°N to 53°S, 100°W to 30°E with a constant horizontal resolution of ⅓°. The vertical structure of the model consists of a variable-depth mixed layer, and a number of layers below the mixed layer specified according to a sigma-coordinate system. The mixed layer depth and thickness of the deepest sigma layer are computed prognostically and the remaining layers are computed diagnostically such that the ratio of each sigma layer to the total depth below the mixed layer is held to prescribed values. In this study, the ocean is divided into 20 layers, with an initial mixed layer depth determined from the *World Ocean Atlas 2001* (WOA) climatology (Conkright et al. 2002) according to a prescribed density criterion in which $\Delta\sigma = 0.125$ kg m^{-3} (Kara et al. 2000). The active model of the reduced-gravity ocean is bounded below by the $\sigma_\theta = 27.8$ kg m^{-3} isopycnal, associated with the base of the Antarctic Intermediate Water [i.e., the intermediate layer for the South Atlantic (Schmid et al. 2000)]. The thermocline region, contained between the base of this layer and the base of the mixed layer, is divided into the remaining 19 layers. The ratio of the layer depths is chosen according to typical values encountered in the ventilation region of the South Atlantic and ensures high resolution just below the mixed layer and a gradual decrease in resolution toward the model bottom layer.

The horizontal boundary conditions are no slip and no flux. A 10° wide sponge layer is used near the northern and southern boundaries for the purpose of gradually relaxing temperature and salinity toward climatology. The model is initialized with monthly means of temperature, salinity, and layer thickness from the WOA climatology and driven by monthly means of wind stress, solar radiation, precipitation, cloudiness, relative humidity, and sea surface air temperature from COADS climatology (da Silva et al. 1994). The heat fluxes are calculated by the bulk forcing method similar to the one used by Giese and Cayan (1993). A more detailed description of the heat and freshwater fluxes can be found in Kochurov (2002). The model is spun up from rest for 20 yr until it reaches a nearly asymptotic state so that the annual cycle is very similar over the last 5 yr of integration. The results to be analyzed here are the monthly averages taken from the last year of integration.

3. The bifurcation of the southern branch of the South Equatorial Current (sSEC)

a. Observations

There is some observational evidence of the sSEC poleward shift with depth, portrayed as a wedging of the thermocline on the equatorial side of the subtropical gyre (Tsuchiya et al. 1994). However, no detailed description has yet been made of the depth dependence and seasonal variability of the bifurcation of the sSEC, which is the objective of this study. The observations are used here to provide a description of the annual mean depth dependence of the sSEC bifurcation since they are insufficient to resolve its seasonal variability.

Figure 2 shows the annual mean dynamic height and geostrophic flow relative to 1000 dbar, at 0, 100, 200, 400, 600, and 800 m, calculated from the hydrographic observations described in section 2. These maps demonstrate the poleward shift of the sSEC with increasing depth. Near the surface (0–100 m), the sSEC is a broad current confined within the latitude band between 8° and 20°S near the coast and bifurcates at around 14°S (see black circles). At 200 m, the sSEC is confined to the region south of 10°S and bifurcates at 18.6°S. At 400 m, the sSEC flows entirely south of 14°S leaving a broad region of almost no motion to the north; the bifurcation latitude is about 21°S. At 600 and 800 m, a weaker sSEC flows south of 20°S bifurcating at 23.6° and 25.5°S, respectively. The depth dependence of the bifurcation latitude can be seen in more detail in Fig. 3a, which shows the geostrophic meridional velocity averaged within a 2° longitude band off the South American coast. Note that calculations for these maps do not include the Ekman current, which would affect the bifurcation latitude near the surface. Adding the Ekman currents to the geostrophic currents (calculated from observations) moves the bifurcation latitude northward by about 1° [i.e., the bifurcation occurs at 13°S at the surface (not shown)]. The sSEC bifurcation latitude is approximately 26°S at 900 m. Thus, its shift with depth is approximately 7° in the top 400 m and 6° below it according to the observations.

These results agree with the available literature. From hydrographic data, Stramma and England (1999) showed that the bifurcation latitude is 16°S in the near-surface layer (top 100 m), 20°S in the South Atlantic Central Water (SACW) layer (100–500 m), and 26°S in the intermediate layer (500–1200 m). Using isobaric RAFOS floats, Boebel et al. (1999) showed that the Return Current [analog to the SEC, but within the Antarctic Intermediate Water (AAIW) layer] reaches the South American coast at about 28°S (called by the au-thors the Santos Bifurcation). Using data from the World Ocean Circulation Experiment (WOCE) hydrographic section A17 taken during the austral summer of 1994, Wienders et al. (2000) estimated the transport of the SEC and its bifurcation latitude for several isopycnal layers: the SEC bifurcation latitude is 14°S at the surface, 24°S in the 26.7–26.9 σ_θ layer (400–500 m), and nearly constant around 26°–28°S in the AAIW and Upper Circumpolar Water (UCPW: 600–1200 m). (The Wienders et al. results should be interpreted with caution because they are based on a single hydrographic section taken 6°–10° from the western boundary.)

In the annual mean, the poleward shift with depth of the sSEC bifurcation is approximately 14° of latitude in the top 1000 m, in contrast to the shift of its counterpart in the North Pacific, which does not exceed 8° of latitude (Fig. 11 in Qu and Lukas 2003). The presence of the northward upper limb of the MOC in the South Atlantic augments the flow of the equatorward western boundary current. Intermediate water from Cape Basin is still part of the wind-driven subtropical gyre system below 400 m (Schmid et al. 2000) and one-third of it flows northward underneath the BC along with the NBUC (Boebel et al. 1999) to supply part of the water necessary to close the MOC in the Atlantic (also confirmed in this study from particle trajectory analysis, not shown). As the intermediate water flows underneath the BC, it pushes the bifurcation poleward (i.e., southward) below 400 m, increasing the total shift with depth. The situation seems to be reversed in the Pacific NEC region, where the circulation of the South China Sea around the Philippines tends to push the NEC bifurcation equatorward (Metzger and Hurlburt 1996; Qu et al. 2000; Qu and Lukas 2003).

b. Model results

To investigate how well the model simulates the depth dependence of the bifurcation latitude, Fig. 3b shows the annual mean sSEC bifurcation defined as the point where the modeled meridional velocity averaged within a 2° longitude band off the South American coast is zero. In the model, the bifurcation occurs at about 10°–14°S in the top 100 m and shifts poleward with increasing depth, reaching 27°S at 1000 m, similar to the observations (Fig. 3a). The model also seems to reproduce well the latitude–depth distribution of the BC and NBUC. The BC southward flow reaches a maximum of 0.14 m s^{-1} near the surface in both observations and model. The northward NBUC is slightly stronger in the model just south of 5°S (maximum of 0.2 m s^{-1}). The discrepancy between the observed and modeled bifurcation latitude in the top 100 m can only be partially explained in terms of Ekman transport
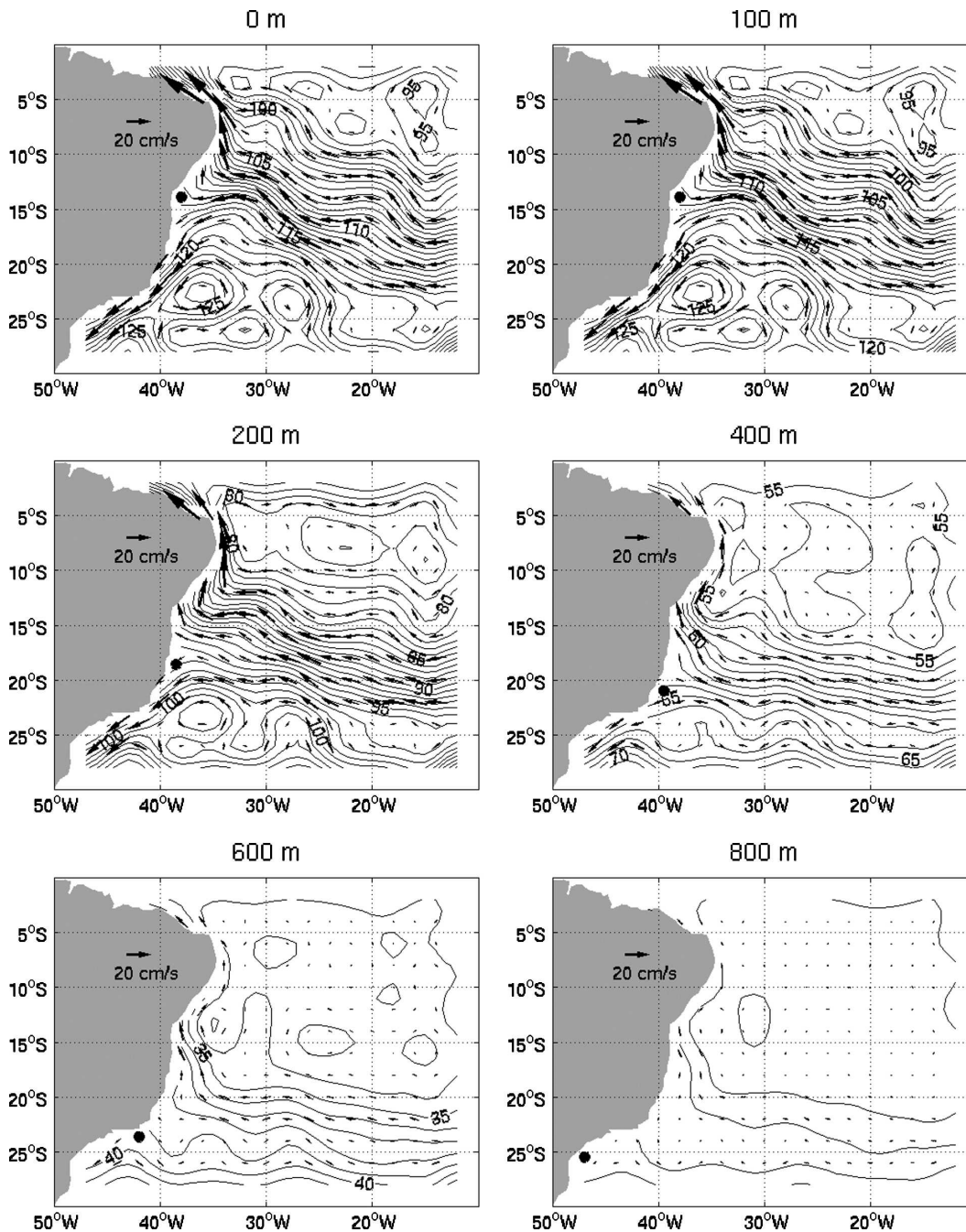
FIG. 2. Annual mean dynamic height ($\times 10^{-1}$ m^2 s^{-2}) and geostrophic flow relative to 1000 dbar at 0, 100, 200, 400, 600, and 800 m. Contour interval: 0.1 m^2 s^{-2}. Black circles represent the location of the sSEC bifurcation.

since adding the Ekman currents to the geostrophic currents moves the bifurcation latitude northward by only 1°. The differences found within the 400–600-m layer are probably due to the model's inability to reproduce accurately part of the ventilation of lower-thermocline waters occurring in the southeast corner of the domain (Cape Basin) near the model artificial boundaries; the coarse horizontal and vertical resolution of the observations may also play a role. Nevertheless, the modeled bifurcation latitude is still within the values published by Stramma and England (1999), Boebel et al. (1999), and Wienders et al. (2000).

The model also reproduces the strength and vertical structure of the currents involved (i.e., NBUC, BC, and
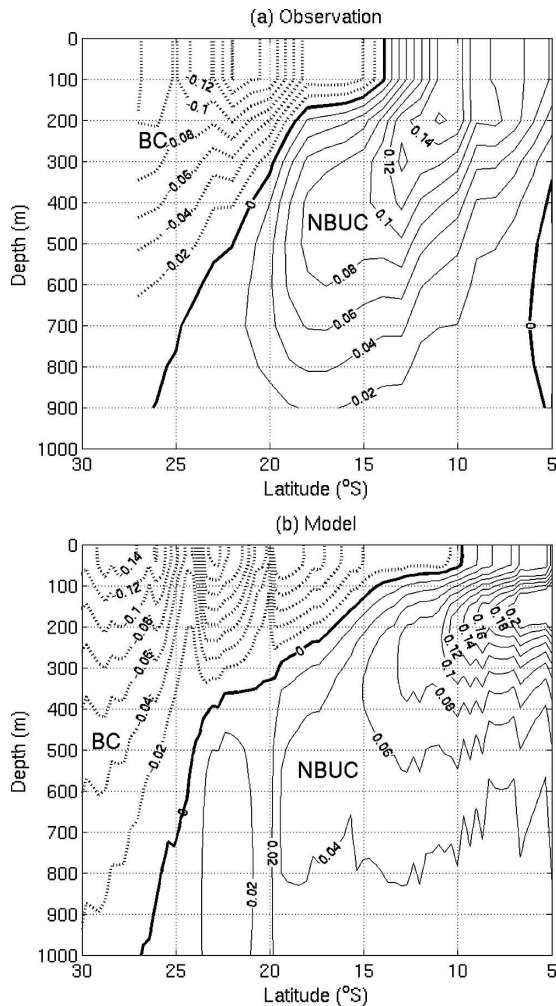
FIG. 3. Annual mean (a) geostrophic meridional velocity from observations and (b) total meridional velocity from the model. The velocities (m s^{-1}) are averaged within a 2° longitude band off the South American coast. Positive (negative) values indicate northward (southward) flow associated with the NBUC (BC), and the contour of zero velocity represents the bifurcation of the sSEC.
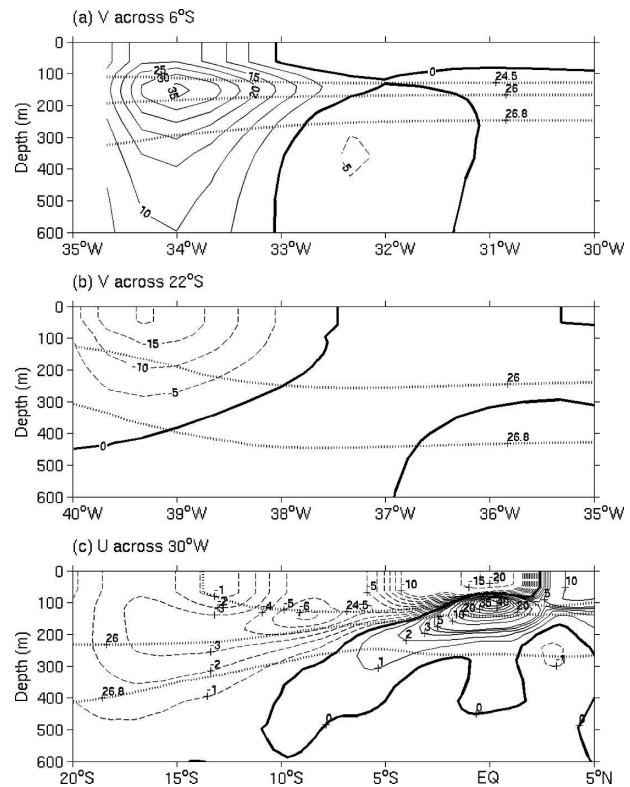

FIG. 4. Vertical section of annual mean meridional velocity (cm s^{-1}) across (a) 6°S and (b) 12°S and zonal velocity across (c) 30°W. Solid (dashed) lines represent positive (negative) values. Contours are every 5 cm s^{-1} in (a) and (b) and every 1 cm s^{-1} for velocities lower than 5 cm s^{-1} and every 5 cm s^{-1} for higher velocities in (c). Gray dotted lines are the 24.5, 26.0, and 26.8 isopycnal surfaces.

SEC). Figures 4 shows vertical sections of meridional velocity along (a) 6°S and (b) 22°S and (c) zonal velocity along 30°W. Dotted lines represent 24.5, 26.0, and 26.8 kg m^{-3} isopycnal surfaces (thermocline layer). The core of the NBUC is located at 100–150 m and reaches velocities of order 0.4 m s^{-1} (Fig. 4a). These results are similar to those published by da Silveira et al. (1994) from hydrographic data; Schott et al. (1995, 2002), however, found core velocities approaching 0.7 m s^{-1} at 5°S in ADCP measurements. Although the model currents are generally weaker than those reported in the literature, the transport estimates agree well with the observations. The modeled NBUC transport is 14 Sv (Sv ≡ 10^6 m^3 s^{-1}) for the top 400 m. Schott et al. (1995, 2002)

estimated respectively 14 Sv and 16 Sv for the NBUC at 5°S above the 26.8 kg m^{-3} isopycnal surface. This is due to the fact that the model NBUC is more diffuse. Most OGCMs fail to reproduce the tightness of the thermocline, in particular in the western boundary and equatorial regions where the structure of the thermocline is very important in determining the strength of the currents (Meehl et al. 2001). This is partially explained by the use of smooth climatologies to initialize and force the models. Moreover, the model results shown so far are annual means and the observational studies use data from snapshots.

The BC at 22°S is confined to the upper 450 m and its core is found at the surface (−0.24 m s^{-1}) (Fig. 4b). Campos et al. (1995) estimated −0.3 m s^{-1} south of 23°S from hydrographic data. The BC transport is 6 Sv for the top 400 m. Garfield (1990) estimated 7 Sv for the top 450 m at 24°S and Campos et al. (1995) 7.3 Sv for the top 750 dbar at 23°S. In Fig. 4c, the SEC is a weak and broad current extending from 20° to 10°S around 400 m, to 5°S around 150 m, and to the north of the

equator at the surface. This is corroborated by Stramma and Schott (1999) and Stramma et al. (2003). The annual-mean westward transport between 6° and 22°S along 30°W for the SEC is estimated to be 18 Sv for the upper 500 m, in good agreement with observations. For instance, Wienders et al. (2000) estimated a westward transport of 21.5 Sv for the SEC within the SACW layer (~500 m) between 7.5° and 20°S, Stramma (1991) estimated 20 Sv for the same region. Note that the model also reproduces well the thermocline depth within the $\sigma_\theta = 24.5$–26.8 kg m^{-3} layer [cf. our Fig. 4 with Figs. 7 and 2 in Schott et al. (1995) and (2002), respectively].

Although the model does not include the barotropic component of the flow, it is still capable of providing the essential vertical structure of the wind-driven gyre circulation. Moreover, by allowing net mass flow in and out of the domain, the use of a sponge layer in the southern and northern boundaries of the domain creates the observed net meridional pressure gradient and associated mass flux between these boundaries, which drives the upper branch of the meridional overturning circulation (Lazar et al. 2002). The numerical simulation gives a net northward mass transport across the equator of 9 Sv for the upper 500 m and 14 Sv for the upper 1000 m, which is in agreement with values found in full OGCM simulations (Blanke et al. 1999) and with observations (Schmitz 1995). This is confirmed by good agreement between the model and observational estimates of NBUC and SEC transports, which constitute the main conduit for the MOC upper limb.

In terms of the seasonal variability of the NBUC, BC, and sSEC transports, it is difficult to evaluate the performance of the model because of the sparseness of in situ data from the tropical Atlantic, reflecting the lack of observational studies in the region. However, the retroflection of the NBC is one of the most robust seasonally varying features in the tropical Atlantic. Although, the NBC retroflection is not the focus of this study, it is important to point out that the model simulates its seasonal cycle very well. The model reproduces the intensification of the NBC (north of the equator) and a growing extension of the NBC retroflection at the surface as the ITCZ migrates across the equator to its northernmost meridional position (from May to August). At the same time, the North Equatorial Countercurrent (NECC) is initiated in the western part of the basin, carrying retroflected NBC flow into the ocean interior. In January–April, the ITCZ attains its southernmost position, reaching as far as 5°S in the west. As a consequence, the modeled NBC diminishes in strength; the NBC retroflection and NECC in the western basin nearly vanish. This is corroborated by
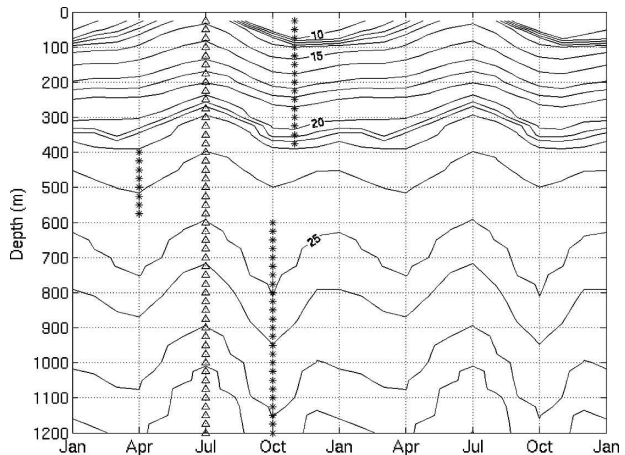

FIG. 5. Time–depth plot of the sSEC bifurcation latitude (°S) determined by the location of zero meridional velocity averaged over a 2° longitude band off the South American coast for each month of the year. Contours are every 1°. Asterisks (triangles) represent the northernmost (southernmost) position of the sSEC bifurcation for each depth.

observational studies (Stramma and Schott 1999) and is investigated in more detail in Rodrigues (2004). The model also simulates the spatial and temporal variations of various isopycnal outcrop lines in the South Atlantic, which are very important in determining subduction of subtropical water and its pathways to the Tropics, more precisely how much water, in which density range, and which months of the year. This is particularly true for the South Atlantic where isopycnal outcrop lines experience a large seasonal range in their positions, as pointed out by Lazar et al. (2002). That was one of the major problems encountered in previous works using the same model (Inui et al. 2002; Lazar et al. 2002). Comparisons of the annual march of the position of several isopycnal outcrop lines from this model and WOA climatology are presented in Rodrigues (2004).

c. Seasonal variability of the sSEC bifurcation and possible mechanisms

To study the seasonal variability of the sSEC bifurcation, the monthly mean meridional velocities from the model are averaged within a 2° longitude band off the coast of South America to determine the zero line for each month. To facilitate comparisons among the different months, Fig. 5 shows a time–depth plot of the bifurcation latitude constructed from the zero meridional velocity line for each month. Asterisks (triangles) represent the northernmost (southernmost) position of the sSEC bifurcation for each depth. Most of the seasonal variability in the bifurcation latitude seems to oc-
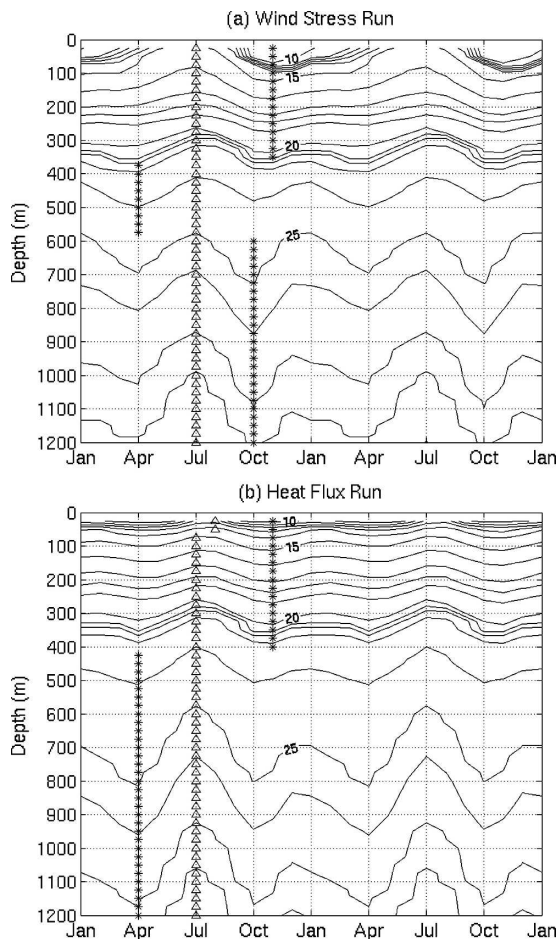
FIG. 6. As in Fig. 5 but for the sensitivity experiments: forced by (a) varying wind stress (WSTR) and (b) varying heat flux (HTFX).
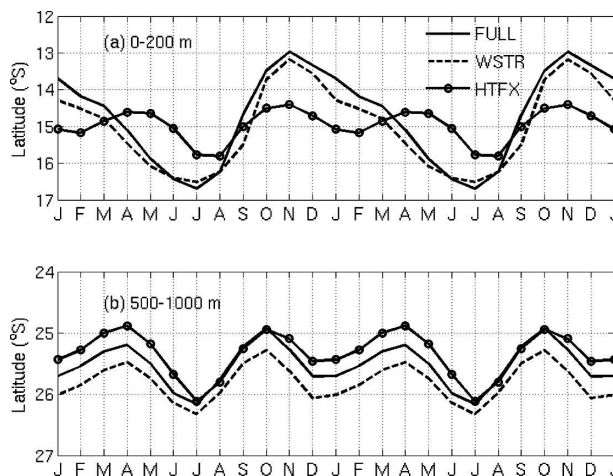

FIG. 7. Seasonal variation of the sSEC bifurcation latitude averaged in (a) the top 200 m and (b) 500–1000 m (bottom) for the full (FULL), WSTR, and HTFX experiments.

cur in the top 400 m, which corresponds roughly to the ventilated thermocline. The bifurcation shifts by 7° of latitude in the top 100 m and by about 3° from 100 down to 400 m. In the unventilated lower thermocline (from 400 to 600 m), the bifurcation varies little during the year (∼1°). Below that, the shift of the bifurcation latitude increases to 2° and the transition from the southernmost to northernmost position does not seem to follow the same pattern as that for the top 400 m.

The mechanisms that determine the seasonal variability of the sSEC bifurcation in the upper thermocline are now investigated. Possible candidates are the atmospheric momentum and heat fluxes. Since the sSEC forms the northern part of the South Atlantic subtropical gyre, which is primarily wind driven, one expects the seasonal variability of the sSEC bifurcation to be related to variations in the wind stress field. Two sensitivity experiments were performed to make sure that this is indeed the case. In the first experiment (called the WSTR run) the model was spun up to a steady

seasonal cycle (20 yr of integration) after having filtered out any seasonality in the heat flux with the atmosphere. This was accomplished by forcing the model with only annual mean values of the atmospheric parameters, with the exception of the wind stress field, which was allowed to vary (monthly mean). In the second experiment (called HTFX) the seasonality in the wind stress field was filtered out and the other atmospheric parameters associated with heat fluxes were allowed to vary.

Time–depth plots of the bifurcation latitude, similar to Fig. 5, were generated for both the WSTR and HTFX sensitivity experiments (Figs. 6a and 6b, respectively). Only small differences can be spotted between the full experiment (FULL, Fig. 5) and the WSTR run. The northernmost and southernmost positions remain the same. On the other hand, the HTFX run shows greater differences, particularly in the top 200 m. Although there is still a seasonal cycle in the latitude bifurcation, it is much weaker in the HTFX run. Even in the 500–1000-m layer the bifurcation latitude varies differently, with the northernmost position occurring in April instead of October. These differences can be seen more clearly in Fig. 7, which shows the seasonal variation of the bifurcation latitude averaged in the (a) 0–200- and (b) 500–1000-m layers for the three experiments. Note that there is a strong annual signal in the variability of the bifurcation latitude in the top 200 m related to the wind stress field (solid and dashed lines in Fig. 7a). When the seasonal cycle in the wind stress is turned off (HTFX), the variability of the bifurcation latitude is dominated by a semiannual signal similar to that in the lower layer between 500 and 1000 m (Fig. 7b). These results confirm that the seasonal variability
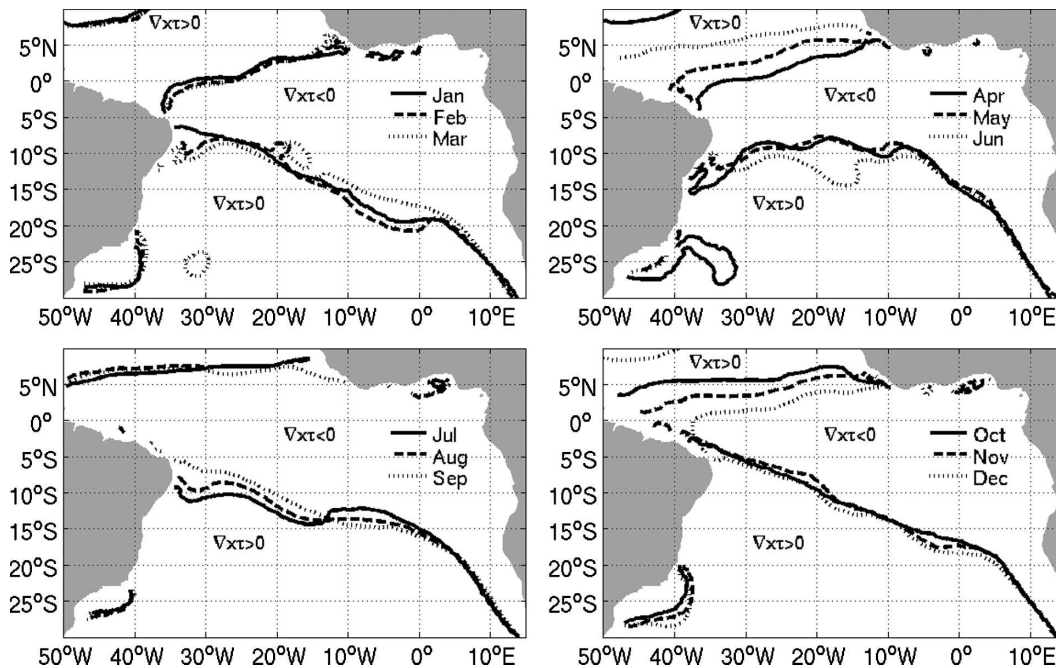
FIG. 8. Zero wind stress curl ($\nabla \times \tau$) line calculated from the COADS monthly climatology (da Silva et al. 1994) used in the model.

of the sSEC bifurcation in the upper thermocline is related primarily to variations in wind forcing by the combined effect of local Ekman pumping and remotely forced Rossby waves.

The seasonal variability of the wind stress curl is now examined. Figure 8 shows the annual migration of the zero wind stress curl line calculated from the COADS monthly mean climatology used in the model. It is possible to observe the meridional excursion of the zero wind stress curl line through the bifurcation region near the South American coast during the year. (This is related to the seasonal meridional movement of the Atlantic marine ITCZ complex.) As a consequence, the bifurcation region is exposed to negative wind stress curl and associated weaker Ekman pumping from February to August and to positive wind stress curl and stronger Ekman suction from September to January. However, the zero wind stress curl line also undergoes a meridional excursion between 20°W and 0°, reaching its northernmost position in May and southernmost in February. It is not clear yet if changes in the wind stress over the bifurcation region are more important that those in the central and eastern side of the basin.

To investigate the importance of local versus remote wind forcing, we performed a lagged cross-correlation analysis between time series of sSEC bifurcation latitude averaged in the top 200 m and the wind stress curl at each grid point (Fig. 9). One expects widespread high correlation coefficients since most signals in the Atlan-

tic are likely to exhibit a semiannual or annual component. However, only in the shaded areas are the correlation coefficients statistically significant at the 99% confidence level. The number of degrees of freedom was estimated according to the independence time scale of Davis (1976), derived from the first zero crossing of the autocovariance function. The highest positive correlation coefficients are, indeed, found in an area close to the bifurcation region: 5°–10°S, 25°–35°W at zero lag (Fig. 9a), pointing to the importance of local forcing. But two "remote" regions also present significant correlation. The first remote region around 13°–18°S, 7°W–3°E presents maximum correlation when the wind forcing leads by 6 months (Fig. 9b), and the second remote region around 25°–30°S, 5°–12°E presents maximum correlation at zero lag (Fig. 9a).

Figure 10 shows the time series of wind stress curl averaged over these three areas as (a) local forcing and (b) remote areas. The temporal correspondence of the bifurcation latitude with the local wind stress curl (Figs. 7a and 10a) is striking, with cross-correlation higher than 0.9 at zero lag. The local wind stress curl has a minimum (-4×10^{-8} N m^{-3}) in July and a maximum (2×10^{-8} N m^{-3}) in November; the bifurcation reaches its southernmost position in July and northernmost position in November. During the austral spring/summer months local positive wind stress curl produces an anomalous anticyclonic circulation, whose southward component near the western boundary causes the sSEC

(a) Cross-correlation at 0 lag
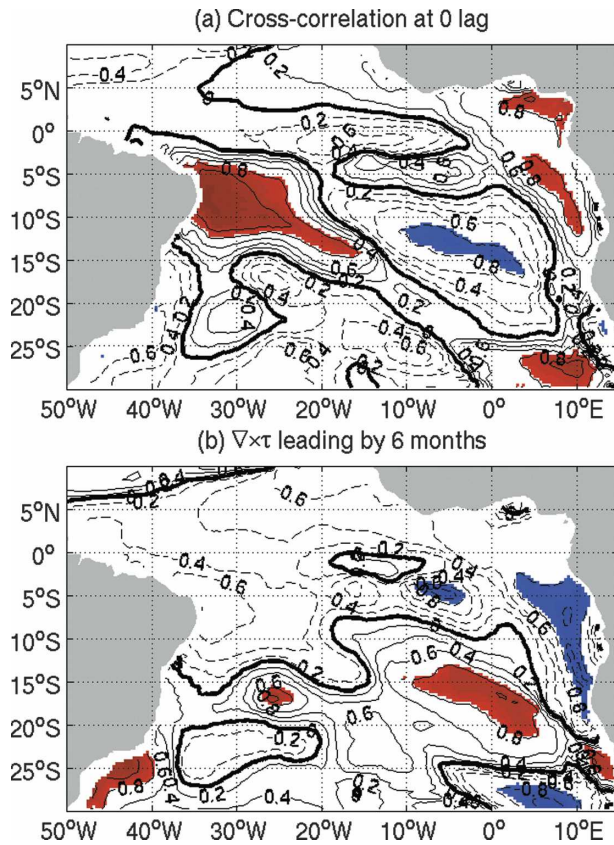

(b) ∇×τ leading by 6 months

FIG. 9. Cross correlation between sSEC bifurcation latitude averaged in the top 200 m (solid line in Fig. 7a) and wind stress curl at each grid point: (a) at zero lag and (b) wind stress curl leading by 6 months. Solid (dashed) lines represent positive (negative) correlation coefficients. Areas where the correlation is statistically significant at the 99% confidence level are shaded. Contours are every 0.2 for correlation coefficients ≤±0.8 and 0.1 for larger-magnitude correlations.

bifurcation to occur at lower latitudes. In contrast, during the austral winter months local negative wind stress curl produces an anomalous cyclonic circulation, and its northward component near the western boundary results in a shift of the sSEC bifurcation to its southernmost position. These anomalous circulations can be seen in Fig. 11, which shows the anomalous flow relative to the annual mean for (a) July and (b) November. Thus, the cyclonic (anticyclonic) circulation caused by negative (positive) wind stress curl makes the southern branch of the cyclonic tropical gyre shift to the south (north) and move the sSEC bifurcation latitude southward (northward). Remember that this anomalous circulation is superimposed on the mean circulation (see Figs. 12a,b for the total flow in July and November).

The split of the SEC into the sSEC and the central branch of the SEC (cSEC) is linked to the anomalous circulation and thus to the local Ekman pumping (cf. Figs. 11 and 12). In July, the anomalous flow weakens
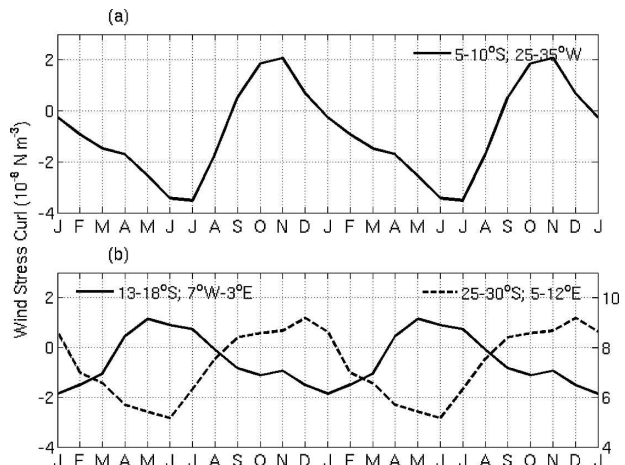

FIG. 10. Seasonal variation of the wind stress curl ($\times 10^{-8}$ N m^{-3}) averaged in the tropical western South Atlantic over the areas where correlation is statistically significant in Fig. 9: (a) 5°–10°S, 25°–40°W; (b) 13°–18°S, 7°W–3°E (solid line); and 25°–30°S, 5°–12°E (dashed line, right y axis). Standard deviations are respectively 1.9, 1.0, and 1.4 $\times 10^{-8}$ N m^{-3}.

the SEC north of 10°S near the coast, making the cSEC flow north of this latitude and the sSEC flow south of it. In November, the SEC split occurs along 12°S, and the anomalous circulation intensifies the cSEC. Note also that the anomalous circulation imposed by the local wind stress in the austral winter months inhibits the interior pathways, thus favoring the communication between the subtropics and Tropics through the western boundary current. On the other hand, in November, with the retreat of the tropical cyclonic gyre, the NBC transport decreases and the interior pathways are favored. When the seasonal variability of the wind stress is not considered (HTFX run), the SEC is a broad constant current all year-round (not shown): the anomalous circulation disappears.

The remote wind forcing is investigated through changes in thermocline depth since they are associated with the meridional movement of the sSEC bifurcation. Negative (positive) wind stress curl shoals (deepens) the thermocline, producing the anomalous cyclonic (anticyclonic) circulation in July (November) that results in the shift of the sSEC bifurcation to its southernmost (northernmost) position. Figure 13 shows Hovmöller phase diagrams of the anomalies of the depth of the 26.0 isopycnal with respect to the annual mean along (a) 8°, (b) 10°, (c) 12°, and (d) 14°S. These latitudes were chosen because the strongest anomalous currents in the western boundary are confined to this latitude range (see Fig. 11). The 26.0 isopycnal surface represents roughly the core of the thermocline layer in the South Atlantic (Fig. 4). A careful look at the annual march of the thermocline depth anomalies suggests
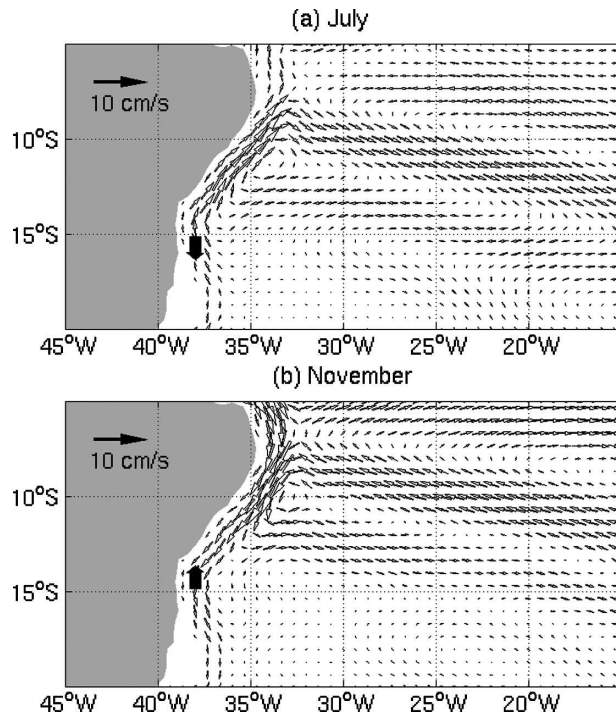
FIG. 11. Anomalous flow (cm s^{-1}) at 100 m relative to the annual mean field for (a) July and (b) November. The thick arrows illustrate the shift of the sSEC bifurcation at 100 m.

FIG. 12. Modeled velocity field (cm s^{-1}) at 100 m for (a) July and (b) November.

that, indeed, local forcing is crucial in determining the seasonal variability of the bifurcation latitude and associated thermocline depth anomalies in that region. Stronger anomalies are confined to the west of 25°W along 8°, 10°, and 12°S. Anomalies with opposed phases are generated east of 20°W, but they are weaker. It is clear from the time series of the wind stress curl averaged over the local and remote central regions (black lines in Figs. 10a,b) that their signals are in approximate quadrature, the remote being weaker (half amplitude of the local). Interestingly, the weak negative anomalies, generated in the middle of the basin along 12°S during austral summer, travel westward with speeds around 0.1–0.2 m s^{-1} (approximately first baroclinic mode speed), reaching the western boundary during the austral winter, enhancing the locally generated anomalies. This is consistent with the lagged cross correlation with maximum correlation occurring at zero and 6-month lag for the local and remote regions, respectively. Along 14°S, stronger anomalies are centered at 20°W, but do not reach the western boundary. Anomalies generated east of 0° also do not reach the western part of the basin. The remote forcing (i.e., westward propagation of anomalies) appears to have an enhancing effect, albeit weak, on the seasonal variability of the bifurcation in the upper thermocline.

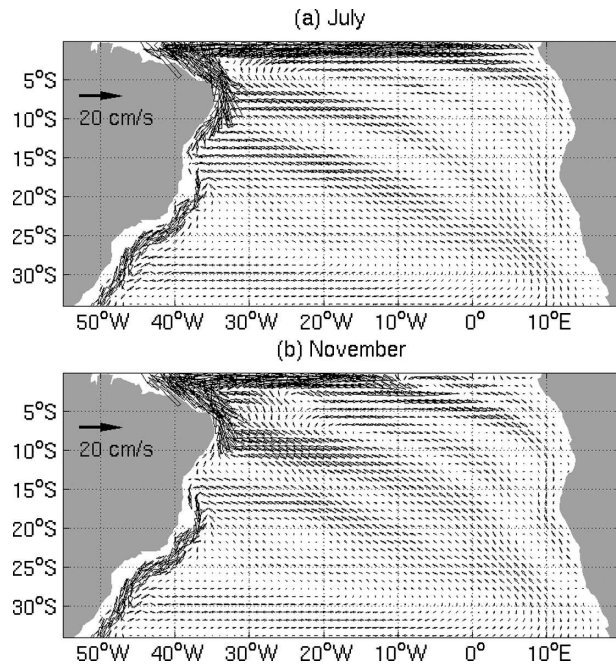Although the variability of the depth of the isopycnal surfaces within the upper thermocline (or, equivalently, sea level) in the western South Atlantic reflects, in principle, the integrated effect of the wind stress curl across the basin, the wind stress curl anomaly over the western part of the basin near 5°–10°S is larger than that in the middle and eastern part (standard deviations of 1.9, 1.0, and 1.4 × 10^{-8} N m^{-3}, respectively) so the upper-thermocline flow around the bifurcation region is largely locally forced. Moreover, the variations in upper-thermocline depth and circulation (Figs. 13 and 11) correspond with those of the local wind stress curl (Fig. 10a), indicating that local wind stress curl anomalies near 5°–10°S modify the strength of the horizontal circulation to create a counteracting tendency of boundary and interior transports in the upper thermocline (see Fig. 11). This counteracting tendency was studied by Lee and Fukumori (2003) at 10° latitude in the North and South Pacific. They found similar results: the variability of the sea level and pycnocline flow in the western Pacific is largely forced by changes in the local wind stress curl. Though the horizontal scale of the forcing is greater and the time scale of the adjustment longer in the Pacific. Along 10°N in the Atlantic, da Silva and Chang (2004) showed that the thermocline displacement and poleward flow in the western part of the basin (west of 45°W) are mainly controlled by local Ekman pumping on seasonal time scales, whereas Rossby wave adjustment is important in the interior and eastern part of the basin.
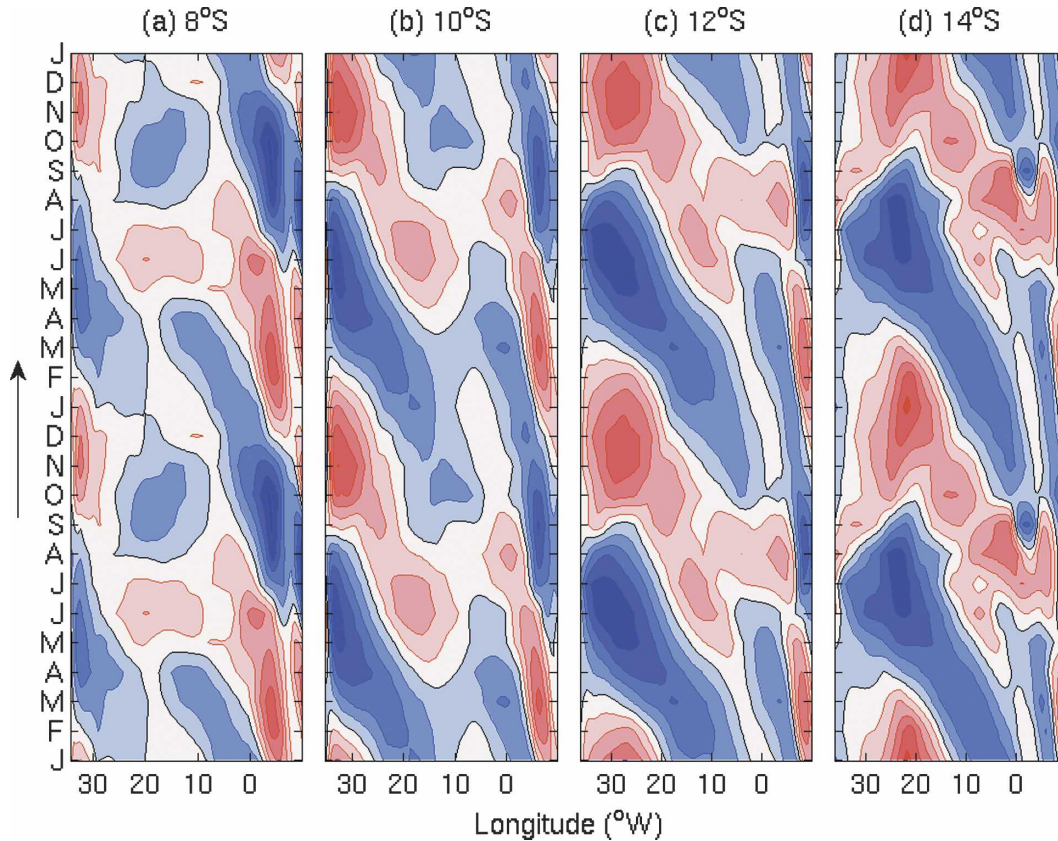
FIG. 13. Depth anomaly of the $\sigma_\theta = 26.0$ isopycnal relative to the annual mean. Blue (red) shades represent negative (positive) values. Contours are every 2 m. For reference, the mean isopycnal depth is 110, 120, 130, 140 m along 8°, 10°, 12°, and 14°S, respectively.

Qu and Lukas (2003) found similar results for the Pacific NEC: the seasonal variability of its bifurcation latitude is determined in great part by the local Ekman pumping. In the Atlantic, interestingly, the transition from the northernmost to the southernmost position of the marine ITCZ complex and vice versa is uneven in time, with the former taking 4 months and the latter 8 months. This uneven pattern in the forcing is reflected in the seasonal variability of the sSEC bifurcation. Conversely in the Pacific, the peak-to-peak timing of the meridional excursion of the ITCZ is even, and so is that of the seasonal variability of the NEC bifurcation latitude (cf. their Fig. 7 with our Figs. 7a and 10a).

Figure 14a shows the volume transports of the SEC, BC, and NBUC, integrated from the surface to 400 m along 30°W (6°–22°S) for the SEC, along 22°S (from the coast to 37.5°W) for the BC, and along 6°S (35°–32°W) for the NBUC (see transect locations in Fig. 1). The SEC, BC, and NBUC each have peak-to-peak variability of about 2–3 Sv. The SEC has a mean westward transport of 15 Sv, the BC a mean southward transport
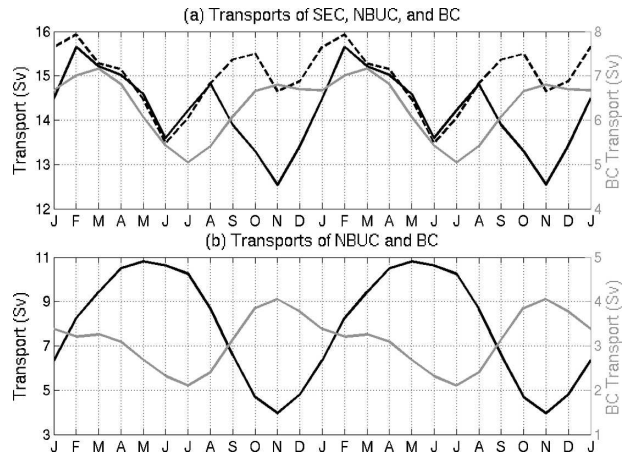
FIG. 14. Seasonal variability of (a) the South Equatorial Current (SEC) along 30°W (black dashed line), the North Brazil Undercurrent (NBUC) along 6°S (black solid line), and the Brazil Curent (BC) along 22°S (gray solid line) and (b) the NBUC along 10°S (black solid line) and the BC along 18°S (gray solid line). Positive values represent westward transport for the SEC, northward for the NBUC, and southward for the BC (right y axis).

of 6 Sv, and the NBUC a mean northward transport of 14 Sv. These values agree well with the literature (section 3a). For instance Schott et al. (1998) found an average transport of 14.6 Sv for the NBUC across 5°S; Stramma and Peterson (1990) found 16 Sv for the SEC across 30°W (upper 400 m), and 4 Sv for the BC across 15°S. Since the bifurcation latitude variability is a manifestation of changes in the flow of the currents involved, the local component of the forcing (Fig. 10a), responsible for most of the variability in the sSEC bifurcation, explains the decrease in the transport of both SEC and BC in June and July and the subsequent increase in September–November. The relationship between the bifurcation location and the transport of the currents involved is more obvious if one analyzes the variability of the latter closer to the bifurcation latitude, for instance the transports of the NBUC along 10°S and BC along 18°S (Fig. 14b). As the sSEC bifurcates in its southernmost (northernmost) position in June–July (October–November), the NBUC transport increases (decreases) and the BC transport decreases (increases). Note that the seasonal cycle of the NBUC transport is very sensitive to latitude: at 10°S the maximum transport is achieved during the austral fall/winter months (April–July), whereas at 6°S the maximum transport happens during summer. The difference between the NBUC transports along 6° and 10°S reaches its minimum of 3 Sv in June–July when the cSEC weakens and the sSEC bifurcation is in its southernmost position. Conversely, this transport difference reaches its maximum of 8 Sv in October–November when the cSEC intensifies and the sSEC bifurcation is in its northernmost position.

Overall, the local forcing appears to exert the main influence on bifurcation position and current transports. These results agree with findings of Stramma et al. (2003) based on hydrographic sections and altimetry data. They showed that only weak remote flow variability is imprinted on the equatorial currents by the sSEC, and the larger variability observed in the NBUC and in the zonal equatorial currents is related to equatorial processes rather than sSEC variability. Our study presents one mechanism for this.

4. Conclusions

In this study, a reduced-gravity, primitive equation ocean circulation model is used to investigate the mean pathways between the South Atlantic subtropical and tropical upper ocean, with emphasis on seasonal variability of the sSEC bifurcation into the BC and NBUC. The model results show good agreement with existing observations, suggesting that the dynamics of the region, including the western boundary currents and zonal tropical current system, are accurately represented in the model.

In the annual mean, the sSEC bifurcation occurs at about 10°–14°S near the surface and shifts poleward with increasing depth, reaching south of 27°S at 1000 m. Seasonal variability of the bifurcation latitude is strongest in the top 400 m, where it reaches its southernmost position in July and northernmost position in November. The bifurcation latitude varies by 7° in the top 100 m, by about 3° from 100 m down to 400 m, by less than 1° between 400 m and 600 m, and 2° below 600 m.

Seasonal variability in the upper thermocline is strongly related to the local wind forcing. Local positive (negative) wind stress curl produces an anomalous anticyclonic (cyclonic) circulation, whose southward (northward) component near the western boundary causes the sSEC bifurcation to occur at lower (higher) latitude during the austral spring/summer (winter) months. Variability in the amplitude of local wind stress curl is due to the annual north–south excursion of the marine ITCZ complex. There is a change in depth of the thermocline in the bifurcation region associated with the aforementioned process. The local component of the forcing, responsible for most of the variability in the sSEC bifurcation, explains the decrease in the transport of both the SEC and BC in June and July and the subsequent increase from September to November. When the sSEC bifurcation moves southward (northward), the NBUC transport increases (decreases) and the BC transport decreases (increases). The remote wind forcing enhances the local response.

These results can potentially have important implications on the subtropical–tropical water exchange and consequently on climate. Theoretical studies of the subtropical–tropical connections have hypothesized that the water pathways between the subtropics and Tropics (or shallow overturning circulation) are determined mainly by the ocean–atmosphere fluxes in the subtropical subduction zones (McCreary and Lu 1994; Lu and McCreary 1995; Liu et al. 1994; Kleeman et al. 1999). Most of the exchange in the tropical Atlantic takes place in the upper thermocline (23.5–26.2 kg m^{-3} layer) west of 20°W in the Southern Hemisphere (Zhang et al. 2003). This study shows that the upper thermocline circulation in the region is strongly affected by variability of the tropical wind stress field (5°–15°S, 35°W–0°), at least on seasonal time scales. The effects of local wind stress on the SEC branches are particularly important because, by changing their paths, water masses are exposed to different surface fluxes and mixing. This, in turn, can alter their properties in a variety of ways.

Studies of the tropical Pacific have already demon-

strated the importance of the variability of the tropical wind stress field in regulating tropical SSTs by changing the strength of the shallow overturning circulation at interannual to decadal scales (Nonaka et al. 2002; McPhaden and Zhang 2002, 2004). Moreover, a similar relationship between variations of bifurcation latitude and current transports was found in the North Pacific on interannual time scales (Kim et al. 2004). Therefore, the mechanisms discussed here, responsible for the seasonal variability of the sSEC bifurcation and the transports of the involved currents (SEC, BC, and NBUC), are plausibly the same as those responsible for interannual variability.

In the future, a detailed climatology should be constructed from all available historical hydrographic data to investigate the seasonal variability of the sSEC bifurcation from observations. At present, this study does not consider the effects of MOC variability and tropical instability waves. Since MOC variability occurs on longer time scales, it should have little impact on the seasonal variability of the bifurcation. However, the use of a full OGCM with higher horizontal resolution that simulates the MOC and its variability would provide a more complete picture of the bifurcation. A study of interannual variability of the sSEC bifurcation is under way.

REFERENCES

Blanke, B., M. Arhan, G. Madec, and S. Roche, 1999: Warm water paths in the equatorial Atlantic as diagnosed with a general circulation model. *J. Phys. Oceanogr.,* **29,** 2753–2768.

Boebel, O., R. E. Davis, M. Ollitrault, R. G. Peterson, P. L. Richardson, C. Schmid, and W. Zenk, 1999: The intermediate depth circulation of the western South Atlantic. *Geophys. Res. Lett.,* **26,** 3329–3332.

Campos, E. J. D., J. E. Gonçalves, and Y. Ikeda, 1995: Water mass characteristics and geostrophic circulation in the South Brazil Bight: Summer of 1991. *J. Geophys. Res.,* **100,** 18 537–18 550.

Chen, D., A. J. Busalacchi, and L. M. Rothstein, 1994a: The roles of vertical mixing, solar radiation, and wind stress in a model simulation of the sea surface temperature seasonal cycle in the tropical Pacific Ocean. *J. Geophys. Res.,* **99,** 20 345–20 359.

——, L. M. Rothstein, and A. J. Busalacchi, 1994b: A hybrid vertical mixing scheme and its application to tropical ocean models. *J. Phys. Oceanogr.,* **24,** 2156–2179.

Conkright, M. E., R. A. Locarnini, H. E. Garcia, T. D. O'Brien, T. P. Boyer, C. Stephens, and J. I. Antonov, 2002: *World Ocean Atlas 2001: Objective Analyses, Data Statistics, and Figures.* CD-ROM Documentation. National Oceanographic Data Center, 17 pp.

Curry, R. G., 1996: Hydrobase: A database of hydrographic stations and tools for climatological analysis. Woods Hole Oceanographic Institute Tech. Rep. 96-01, 50 pp.

da Silva, A. M., C. C. Young, and S. Levitus, 1994: *Algorithms and Procedures.* Vol. 1, *Atlas of Surface Marine Data,* NOAA Atlas NESDIS 6, 83 pp.

da Silva, M. P., and P. Chang, 2004: Seasonal variation of the subtropical/tropical pathways in the Atlantic Ocean from a Ocean Data Assimilation Experiment. *Earth's Climate: The Ocean–Atmosphere Interaction, Geophys. Monogr.,* Vol. 147, Amer. Geophys. Union, 305–318.

da Silveira, I. C. A., L. B. de Miranda, and W. S. Brown, 1994: On the origins of the North Brazil Current. *J. Geophys. Res.,* **99,** 22 501–22 512.

Davis, R. E., 1976: Predictability of sea surface temperature and sea level pressure anomalies over the North Pacific Ocean. *J. Phys. Oceanogr.,* **6,** 249–266.

Ganachaud, A., 2003: Large-scale mass transports, water mass formation, and diffusivities estimated from World Ocean Circulation Experiment (WOCE) hydrographic data. *J. Geophys. Res.,* **108,** 3213, doi:10.1029/2002JC001565.

Garfield, N., III, 1990: The Brazil Current at subtropical latitudes. Ph.D. dissertation, University of Rhode Island, 132 pp.

Gent, P., and M. A. Cane, 1989: A reduced gravity, primitive equation model of upper equatorial ocean. *J. Comput. Phys.,* **81,** 444–480.

Giese, B. S., and D. R. Cayan, 1993: Surface heat flux parameterizations and tropical Pacific sea surface temperature simulations. *J. Geophys. Res.,* **98,** 6979–6989.

Ginis, I., R. A. Richardson, and L. M. Rothstein, 1998: Design of a multiply nested primitive equation ocean model. *Mon. Wea. Rev.,* **126,** 1054–1079.

Goes, M., R. Molinari, I. da Silveira, and I. Wainer, 2005: Retroflections of the North Brazil Current during February 2002. *Deep-Sea Res.,* **52,** 647–667.

Harper, S., 2000: Thermocline ventilation and pathways of tropical-subtropical water mass exchange. *Tellus,* **52A,** 330–345.

Hazeleger, W., P. de Vries, and Y. Friocourt, 2003: Sources of the equatorial undercurrent in the Atlantic in a high-resolution ocean model. *J. Phys. Oceanogr.,* **33,** 677–693.

Inui, T., A. Lazar, P. Malanotte-Rizzoli, and A. Busalacchi, 2002: Wind stress effects on subsurface pathways from the subtropical to tropical Atlantic. *J. Phys. Oceanogr.,* **32,** 2257–2276.

Johns, W. E., R. Zantopp, and G. Goni, 2003: Cross-gyre transport by North Brazil Current rings. *Interhemispheric Water Exchange in the Atlantic Ocean,* G. J. Goni and P. Malanotte-Rizzoli, Eds., Elsevier, 411–441.

Kara, A. B., P. A. Rochford, and H. E. Hurlburt, 2000: Efficient and accurate bulk parameterizations of air–sea fluxes for use in general circulation models. *J. Atmos. Oceanic Technol.,* **17,** 1421–1438.

Kim, Y. Y., T. Qu, T. Jensen, T. Miyama, H. Mitsudera, H. W. Kang, and A. Ishida, 2004: Seasonal and interannual variations of the North Equatorial Current bifurcation in a high-resolution OGCM. *J. Geophys. Res.,* **109,** C03040, doi:10.1029/2003JC002013.

Kleeman, R., J. P. McCreary, and B. A. Klinger, 1999: A mecha-

nism for generating ENSO decadal variability. *Geophys. Res. Lett.,* **26,** 1743–1746.

Kochurov, A. G., 2002: The ocean response to atmospheric intraseasonal variability in the tropical Pacific Ocean. Ph.D. dissertation, University of Rhode Island, 228 pp.

Kraus, E. B., and J. S. Turner, 1967: A one-dimensional model of the seasonal thermocline. *Tellus,* **19,** 98–105.

Lazar, A., R. Murtugudde, and A. J. Busalacchi, 2001: A model study of temperature anomaly propagation from the subtropics to Tropics within the South Atlantic thermocline. *Geophys. Res. Lett.,* **28,** 1271–1274.

——, T. Inui, P. Malanotte-Rizzoli, A. J. Busalacchi, L. Wang, and R. Murtugudde, 2002: Seasonality of the ventilation of the tropical Atlantic thermocline in an ocean general circulation model. *J. Geophys. Res.,* **107,** 3104, doi:10.1029/2000JC000667.

Lee, T., and I. Fukumori, 2003: Interannual-to-decadal variations of tropical–subtropical exchange in the Pacific Ocean: Boundary versus interior pycnocline transports. *J. Climate,* **16,** 4022–4042.

Liu, Z., S. G. H. Philander, and R. C. Pacanowski, 1994: A GCM study of tropical–subtropical upper-ocean water exchange. *J. Phys. Oceanogr.,* **24,** 2606–2623.

Lu, P., and J. J. McCreary, 1995: Influence of the ITCZ on the flow of thermocline water from the subtropical to the equatorial Pacific Ocean. *J. Phys. Oceanogr.,* **25,** 3076–3088.

Lumpkin, R., and K. Speer, 2003: Large-scale vertical and horizontal circulation in the North Atlantic Ocean. *J. Phys. Oceanogr.,* **33,** 1902–1920.

Malanotte-Rizzoli, P., K. Hedstrom, H. Arango, and D. B. Haidvogel, 2000: Water mass pathways between the subtropical and tropical ocean in a climatological simulation of the North Atlantic Ocean circulation. *Dyn. Atmos. Oceans,* **32,** 331–371.

McCreary, J. J., and P. Lu, 1994: Interaction between the subtropical and equatorial ocean circulations: The subtropical cell. *J. Phys. Oceanogr.,* **24,** 466–497.

McPhaden, M. J., and D. Zhang, 2002: Slowdown of the meridional overturning circulation in the upper Pacific Ocean. *Nature,* **415,** 603–608.

——, and ——, 2004: Pacific Ocean circulation rebounds. *Geophys. Res. Lett.,* **31,** L18301, doi:10.1029/2004GL020727.

Meehl, G. A., P. R. Gent, J. M. Arblaster, B. L. Otto-Bliesner, E. C. Brady, and A. Craig, 2001: Factors that affect the amplitude of El Niño in global coupled climate models. *Climate Dyn.,* **17,** 515–526.

Metcalf, W. G., and M. Stalcup, 1967: Origins of the Atlantic Equatorial Undercurrent. *J. Geophys. Res.,* **72,** 4959–4975.

Metzger, J. P., and H. E. Hurlburt, 1996: Coupled dynamics of the South China Sea, the Sulu Sea, and the Pacific Ocean. *J. Geophys. Res.,* **101,** 12 331–12 352.

Nonaka, M., S. P. Xie, and J. P. McCreary, 2002: Decadal variations in the subtropical cells and equatorial Pacific SST. *Geophys. Res. Lett.,* **29,** 1116, doi:10.1029/2001GL013717.

Price, J. F., R. A. Weller, and R. Pinkel, 1986: Diurnal cycling: Observations and models of the upper ocean response to diurnal heating, cooling, and wind mixing. *J. Geophys. Res.,* **91,** 8411–8427.

Qiu, B., and R. Lukas, 1996: Seasonal and interannual variability of the North Equatorial Current, the Mindanao Current, and the Kuroshio along the Pacific western boundary. *J. Geophys. Res.,* **101,** 12 315–12 330.

Qu, T., and R. Lukas, 2003: The bifurcation of the North Equatorial Current in the Pacific. *J. Phys. Oceanogr.,* **33,** 5–18.

——, H. Mitsudera, and T. Yamagata, 2000: Intrusion of the North Pacific waters into the South China Sea. *J. Geophys. Res.,* **105,** 6415–6424.

Rodrigues, R. R., 2004: An observational and numerical study of the South Atlantic circulation. Ph.D. dissertation, University of Rhode Island, 175 pp.

Rothstein, L. M., R. H. Zhang, A. J. Busalacchi, and D. Chen, 1998: A numerical simulation of the mean water pathways in the subtropical and tropical Pacific Ocean. *J. Phys. Oceanogr.,* **28,** 322–343.

Schmid, C., G. Siedler, and W. Zenk, 2000: Dynamics of intermediate water circulation in the subtropical South Atlantic. *J. Phys. Oceanogr.,* **30,** 3191–3211.

Schmitz, W. J., Jr., 1995: On the interbasin-scale thermohaline circulation. *Rev. Geophys.,* **33,** 151–173.

Schott, F. A., L. Stramma, and J. Fischer, 1995: The warm water inflow into the western tropical Atlantic boundary regime, spring 1994. *J. Geophys. Res.,* **100,** 24 745–24 760.

——, J. Fischer, and L. Stramma, 1998: Transports and pathways of the upper-layer circulation in the western tropical Atlantic. *J. Phys. Oceanogr.,* **28,** 1904–1928.

——, P. Brandt, M. Hamann, J. Fischer, and L. Stramma, 2002: On the boundary flow off Brazil at 5°–10°S and its connection to the interior tropical Atlantic. *Geophys. Res. Lett.,* **29,** 1840, doi:10.1029/2002GL014786.

Stramma, L., 1991: Geostrophic transport of the South Equatorial Current in the Atlantic. *J. Mar. Res.,* **49,** 281–294.

——, and R. G. Peterson, 1990: The South Atlantic Current. *J. Phys. Oceanogr.,* **20,** 846–859.

——, and M. England, 1999: On the water masses and mean circulation of the South Atlantic Ocean. *J. Geophys. Res.,* **104,** 20 863–20 883.

——, and F. Schott, 1999: The mean flow field of the tropical Atlantic Ocean. *Deep-Sea Res.,* **46,** 279–303.

——, J. Fischer, P. Brandt, and F. A. Schott, 2003: Circulation, variability and near-equatorial meridional flow in the central tropical Atlantic. *Interhemispheric Water Exchange in the Atlantic Ocean,* G. J. Goni and P. Malanotte-Rizzoli, Eds., Elsevier, 1–22.

Talley, L. D., 2003: Shallow, intermediate, and deep overturning components of the global heat budget. *J. Phys. Oceanogr.,* **33,** 530–560.

Tsuchiya, M., L. D. Talley, and M. S. McCartney, 1994: Watermass distributions in the western South Atlantic: A section from South Georgia Island (54°S) northward across the equator. *J. Mar. Res.,* **52,** 55–81.

Vivier, F., and C. Provost, 1999: Direct velocity measurements in the Malvinas Current. *J. Geophys. Res.,* **104,** 21 083–21 103.

Watts, D. R., X. Qian, and K. L. Tracey, 2001: Mapping abyssal current and pressure fields under the meandering Gulf Stream. *J. Atmos. Oceanic Technol.,* **18,** 1052–1067.

Wienders, N., M. Arhan, and H. Mercier, 2000: Circulation at the western boundary of the South and Equatorial Atlantic: Exchanges with the ocean interior. *J. Mar. Res.,* **58,** 1007–1039.

Wilson, W. D., E. Johns, and R. L. Molinari, 1994: Upper layer circulation in the western tropical North Atlantic Ocean during August 1989. *J. Geophys. Res.,* **99,** 22 513–22 523.

Zhang, D., M. J. McPhaden, and W. E. Johns, 2003: Observational evidence for flow between the subtropical and tropical Atlantic: The Atlantic subtropical cells. *J. Phys. Oceanogr.,* **33,** 1783–1797.